Microwave spectroscopy of Josephson junctions in topological superconductors

Pauli Virtanen
O.V. Lounasmaa Laboratory, Aalto University, P.O. Box 15100,FI-00076 AALTO, Finland and Institute for Mathematical Physics, TU Braunschweig, 38106 Braunschweig, Germany

Patrik Recher
Institute for Mathematical Physics, TU Braunschweig, 38106 Braunschweig, Germany

(Dated: March 12, 2013)

We consider microwave spectroscopy of Josephon junctions composed of hybridized Majorana states in topological 1-D superconductors. We point out how spectroscopic features of the junction appear in the current phase relation under microwave irradiation. Moreover, we discuss a way to directly probe the nonequilibrium state associated with the 4π periodic Josephson effect. In particular, we show how the microwave driving can be used to switch from a 4π to a 2π Shapiro step in the current voltage relation.

PACS numbers: 74.45.+c, 71.10.Pm, 73.23.-b

Josephson junctions in topological superconductors differ from conventional superconductor junctions in several fundamental ways. [1–4] Their low-energy Andreev bound state spectrum can generically be well-separated from the continuum spectrum above the superconducting gap. Moreover, the fermion parity structure of the states is different, which is reflected e.g. in wave function overlaps. These differences are due to the bound states being formed through hybridization of Majorana states.

Several distinguishing features of these systems have been proposed, [1, 3, 5–9] and first experimental evidence of the relevant physics was recently obtained in semiconductor nanowires. [10, 11] One major generic feature is the 4π periodic ac Josephson effect. [1] It is a nonequilibrium effect, in which the system retains memory of the population of the bound states during time evolution of the superconducting phase difference $\varphi \mapsto \varphi + 2\pi$. This results to an effective 4π periodic current-phase relation, $I(\varphi) \sim I_c \sin(\varphi/2)$, [1] the consequences of which are visible in Shapiro steps and other observables. [1, 3, 5–7] Importantly, the expected double-frequency Shapiro step feature was recently seen in an experiment [11].

A well-established way to probe the spectrum of a quantum system (e.g. a qubit) is to drive it, and look for resonances as a function of the frequency of the drive. Driving stimulates transitions between energy levels and thereby also induces a nonequilibrium state in the system. This physics is in play in the Andreev bound states in Josephson junctions [12–14] and Majorana wires. [15, 16] Information obtained in this way can also be useful in characterizing the special features of topological superconductor junctions. For instance, a 4π periodic Josephson effect is not necessarily of a topological origin, [17] even though it is a strong indication of it, but combined with additional knowledge of the spectrum its accidental occurrence can be excluded.

Here, we suggest how microwave driving can be used as a separate control parameter for tuning the magnitude of the 4π periodic Josephson current, which does not require crossing topological transitions and thereby adjusting the level structure of the system, which may complicate interpretation of the results. We also discuss how the level structure of the junction is spectroscopically reflected in the dc current in phase- and current-biased situations.

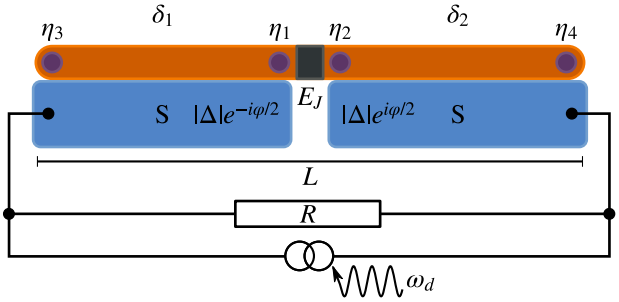

FIG. 1: (Color online) Josephson junction in a 1D (proximity-induced) topological superconductor. The two Majorana states η_1, η_2 located at each side of the junction are hybridized (Josephson energy E_J), whereas the remaining two η_3, η_4 are spatially separated and weakly coupled (coupling energies δ_j). The system is assumed to be current biased and shunted with resistance R (as shown) or phase biased (φ fixed), and driven with a finite frequency ω_d.

Model. We describe the physics of the Josephson junction in topological superconductor (TJJ) by a Bogoliubov–de-Gennes Hamiltonian $\mathcal{H}_{BdG}(t)$. The time-dependence originates from the time dependence of the superconducting phase $\phi(x,t)$; we assume (see Fig. 1) that to the left of the junction $\phi(x,t) = -\varphi(t)/2$, $x < 0$, and to the right, $\phi(x,t) = \varphi(t)/2$, $x > 0$. Such a Hamiltonian can be conveniently rewritten in the corresponding instantaneous Fock eigenbasis, [18]

$$H = \sum_{n=1}^{N} \epsilon_n(\varphi)(d_n^\dagger d_n - \frac{1}{2}) + \hbar \frac{\mathrm{d}\varphi}{\mathrm{d}t} \sum_{m,n=-N}^{N} M_{mn}(\varphi) d_m^\dagger d_n \,, \tag{1}$$

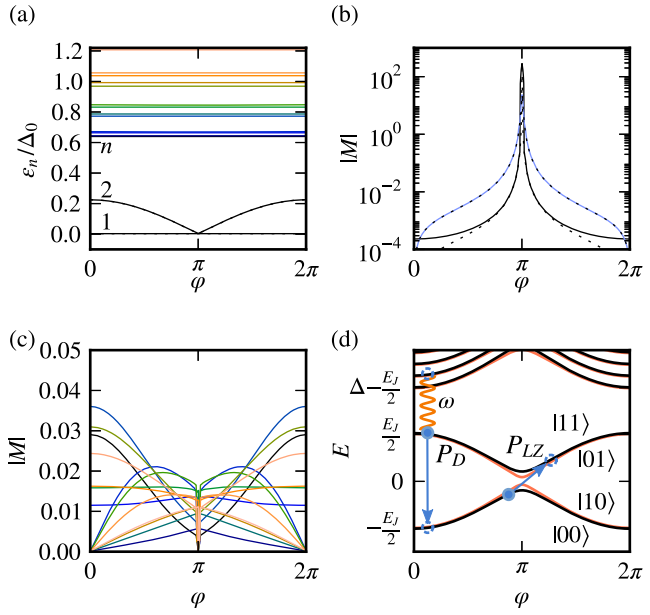

FIG. 2: (Color online) Spectra and connections computed in a Rashba nanowire model. (a) Andreev spectrum ($\epsilon_n > 0$ shown for $n \le 18$). (b) Connections $M_{1,2}$ (black line) and $M_{1,-2}$ (light line) as a function of phase difference. Model connections from Eq. (3) (dotted lines) agree closely with the numerical results. (c) Connections $M_{2,n}$, $2 < n \le 18$ between a low-energy Andreev level and the continuum. The other low-energy level is weakly coupled to the continuum, $|M_{1,n}| \ll |M_{2,n}|$. (d) Schematic many-body spectrum with Landau-Zener (P_{LZ}) and continuum transitions (P_D) indicated. Here, $|n_1 n_2\rangle$ denote the occupation numbers of levels 1 and 2.

where $M_{mn}(\varphi) = -\frac{i}{2}\langle m,\varphi|[\partial_\varphi - i\frac{\hat\tau_3\partial_\varphi\phi}{2}]|n,\varphi\rangle$ are the connections between the instantaneous single-particle eigenstates. $\hat\tau_3$ is the third Pauli matrix (charge density operator) in the electron-hole space, and we choose a basis such that $d_{-n} = d_n^\dagger$, $\epsilon_{-n} = -\epsilon_n$.

The low-energy physics is captured by a model Hamiltonian for the hybridization of the Majorana states, [1]

$$H = iE_J \cos\left(\frac{\varphi}{2}\right)\eta_1\eta_2 + i\delta_1\eta_1\eta_3 + i\delta_2\eta_4\eta_2\,, \qquad (2)$$

where η_j are the four Majorana operators in Fig. 1. The resulting connections are $M_{1,1} = M_{2,2} = 0$, and

$$M_{\pm 2,1}(\varphi) = \frac{E_J}{8}\frac{\delta_\mp}{\delta_\mp^2 + \left(\frac{E_J}{2}\right)^2\cos^2(\varphi/2)}\sin\left(\frac{\varphi}{2}\right)\,, \qquad (3)$$

where $\delta_\pm = \delta_1 \pm \delta_2$. Away from the level crossing at $\varphi = \pi$, these matrix elements are proportional to Majorana state overlaps, which are exponentially small when the length of the wire segments $L/2$ is large compared to the superconducting coherence length $\xi = \hbar v_F/\Delta$.

To compare with a specific microscopic theory, we consider the connections in a semiconductor nanowire model; [4, 7, 19, 20] the results in Figs. 2(a),(b) show how Eqs. (2), (3) capture the low-energy features. [28] The connections to the continuum at $\epsilon > \Delta$ are not exponentially small as shown in Fig. 2(c), and have a relatively weaker dependency on φ. The energy gap $\Delta - E_J$ depends on the transparency of the junction. [2]

Electromagnetic drive couples to the junction by inducing a voltage $V(t) = -(s_d\hbar\omega_d/e)\sin(\omega_d t)$ across the system, equivalent to a superconducting phase difference $\varphi(t) = \frac{2e}{\hbar}\int^t \mathrm{d}t\, V(t) = 2s_d\cos(\omega_d t)$.

We concentrate on the population dynamics of the current-carrying low-energy levels, and treat the coupling to the continuum as a perturbation. [7] For simplicity, we assume the continuum connections M have roughly constant order of magnitude in the relevant energy range around $\pm\epsilon + \hbar\omega_d$ [cf. Fig. 2(c)], that the continuum density of states is steplike, $\mathcal{N}(\epsilon) = \mathcal{N}\theta(|\epsilon| - |\Delta|)$, and that the quasiparticle population in the continuum is negligible. The resulting master equation for the states 1 and 2 is

$$\dot\rho = \mathcal{L}\{\rho\} = -i[H_0',\rho] - \sum_{kk'=-2}^{2}[A(\epsilon_{k'}) + A(\epsilon_k)^*] \qquad (4)$$
$$\times\left\{d_{k'}P\rho P d_k^\dagger - \frac{1}{2}[d_k^\dagger d_{k'},\rho]_+\right\},$$

$$H_0' = H_0 + \frac{i}{2}\sum_{kk'=1,2}[A(\epsilon_{k'}) - A(\epsilon_k)^*]d_k^\dagger d_{k'}\,, \qquad (5)$$

$$A(\epsilon) \approx i\hbar\Gamma_D\log\left(\frac{(\hbar\omega_d)^2 - (\epsilon - \Delta + i\frac{\hbar\Gamma_0}{2})^2}{(\hbar\omega_d)^2 - (\epsilon - E_c + i\frac{\hbar\Gamma_0}{2})^2}\right)\,, \qquad (6)$$

where $\Gamma_D = \hbar\mathcal{N}|M|^2 s_d^2\omega_d^2$ is the transition rate, $P = (-1)^{d_1^\dagger d_1 + d_2^\dagger d_2}$ is the Fermion parity, and H_0 the part of Eq. (1) involving only levels 1 and 2. $\mathrm{Re}\,A(\epsilon) \approx \pi\hbar\Gamma_D\theta(|\omega_d| - |\epsilon - \Delta|)$. E_c is a cutoff energy, originating from the fact that $M \sim \epsilon^{-1}$ decays at energies $\epsilon \gg \Delta$; the results below are insensitive to it. Γ_0 is the inverse lifetime of the continuum levels, which are assumed to be better coupled to external leads than the localized low-energy bound states. For $\Delta + \epsilon_2 > \hbar\omega_d > \Delta - \epsilon_2$ [see Fig. 2(d)], the result describes quasiparticles on level 2 absorbing energy from the field and escaping to the continuum, leading to depopulation ("cooling"). [13] The opposite emission process is limited by the low quasiparticle population in the continuum.

Current-phase relation. Consider first the phase biasing condition, $\varphi(t) = \phi_0 + 2s_d\cos(\omega_d t)$, in which the DC part ϕ_0 is kept fixed. In this setup, 4π periodic nonequilibrium effects are not visible, but one can study spectroscopic features of the junction.

We augment Eq. (4) with quasiparticle poisoning (parity non-conserving), relaxation (parity-conserving), and dephasing described by phenomenological rates, for which we assume values $\Gamma_q, \Gamma_r \sim 10^{-4}E_J/\hbar$ and $\Gamma_d \sim 10^{-3}E_J/\hbar$, respectively. [7, 21, 22] Resulting DC current $\overline{\langle\partial_\varphi H\rangle}$ is shown in Fig. 3. As in quantum point

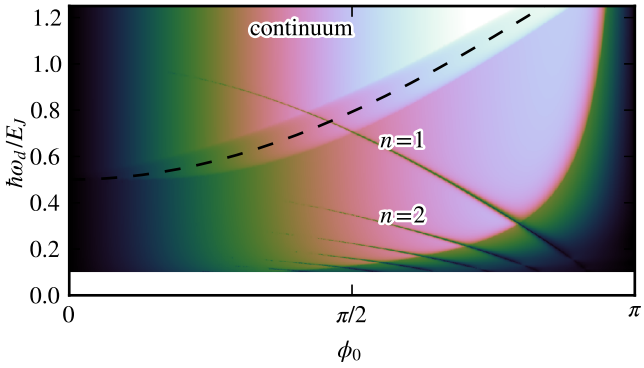

FIG. 3: (Color online) Time-averaged current-phase relation $\bar{I}(\phi_0)$ as a function of excitation frequency ω_d, keeping AC amplitude fixed at $\hbar s_d \omega_d = 0.1 E_J$ and $\Gamma_D = 10^{-5} E_J$ (lighter color: larger current). We take $\Delta/E_J = 1.5$ and $\delta_+/E_J = 10^{-2}$, $\delta_-/E_J = 10^{-3}$. The dashed line indicates the threshold $\hbar\omega_d = \Delta - \epsilon_2(\varphi)$ for continuum transitions. The n-photon resonances $n\hbar\omega_d = \epsilon_2(\varphi) - \epsilon_1(\varphi)$ between the Andreev bound states for $n = 1, 2$ are indicated. The frequency-dependent threshold near $\varphi = \pi$ is due to LZ transitions, which play a role when $\phi_0 + 2s_d > \pi$.

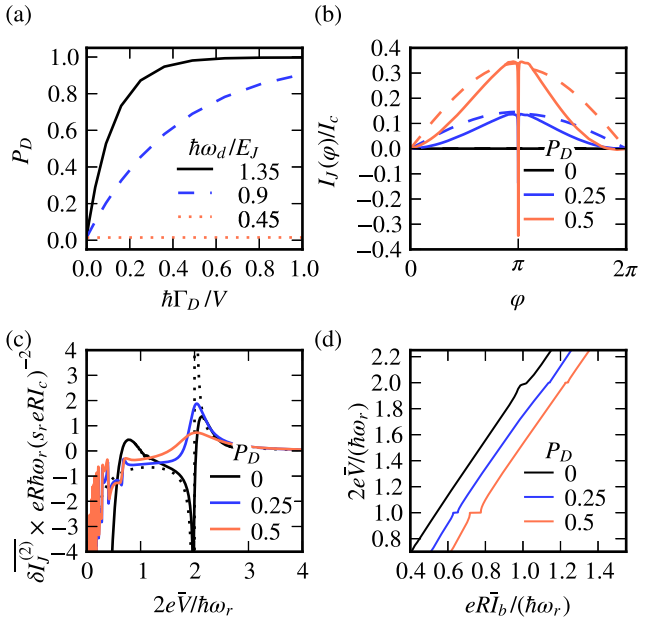

FIG. 4: (Color online) Tuning the 4π periodic Josephson effect. (a) Relationship between the effective parameter P_D and the microscopic model, for $\Delta = 1.5 E_J$ and $\bar{V} \gg \Gamma_{q,r}$, δ^2/E_J. (b) Effective current-phase relation, as obtained from master equation Eq. (4) with $\hbar\omega_d/E_J = 1.35$ (solid lines), and the analytical result Eq. (10) with P_D from Fig. 4(a) (dashed lines). (c) The 4π Shapiro kink for $P_{LZ} = 1$ and $P_D = 0, 0.25, 0.5$ from Eq. (8). For $P_D = 0$ the result is shown as a dotted line; the solid line indicates an exact result without the mean-field approximation. (d) Composite result from Fig. 4(c) and Eq. (10) for the Shapiro steps with parameters $RI_c/(\hbar\omega_r) = 0.2$, $s_r \equiv RI_r/(\hbar\omega_r) = 0.5$, $P_{LZ} = 1$ and different P_D. The curves are offset horizontally for clarity.

contacts [13], resonant transitions can here be identified with sharp dips in the current-phase relation at n-photon resonances $n\hbar\omega_d = \epsilon_2(\varphi) - \epsilon_1(\varphi)$. The transition rate is proportional to the connections $M \sim \delta/E_J$ (forbidden [4] if there is no overlap, $\delta_{1/2} = 0$), but it is balanced against the small rates Γ_q and Γ_r. The second apparent feature is that at $\Delta + \epsilon_2(\varphi) > \hbar\omega_d > \Delta - \epsilon_2(\varphi)$, the transitions to continuum [13] depopulate level 2 and thereby increase the current. Note that in conventional quantum point contacts, the continuum excitation gap $\Delta - \epsilon_2$ is zero at $\varphi = 0$, whereas here it remains finite for all φ, reflecting the qualitatively different energy spectrum.

Tuning the 4π periodic Josephson effect. The 4π periodic Josephson effect [1, 2] under dc bias $\varphi(t) = 2e\bar{V}t/\hbar$ in this system requires (i) Landau-Zener (LZ) transitions at $\varphi(t) = \pi + 2\pi n$ and (ii) a large gap between the continuum and bound state spectra [see Fig. 2(d)], which allows correlations between φ and $\varphi + 2\pi$ be preserved. The former requires a transition probability $P_{LZ} \simeq e^{-8\pi\delta^2/(E_J\bar{V})} \approx 1$. [5] The latter can be modified through the "cooling" effect discussed above. An additional high-frequency signal $\Delta + E_J > \hbar\omega_d > \Delta - E_J$ causes a transition to the lower-energy states with probability $P_D > 0$ during a cycle from $\varphi = 2\pi n - \pi$ to $\varphi = 2\pi n + \pi$.

The probability P_D can be found by considering the time evolution of Eq. (4) in the voltage-biased case. Given initial condition $\rho(t_1) = |11\rangle\langle 11|$ (or $|01\rangle\langle 01|$) at $\varphi(t_1) = -\pi + \beta$, at $\varphi(t_2) = \pi - \beta$ we have $P_D = 1 - \rho_{01,01}(t_2) - \rho_{11,11}(t_2)$, which is shown in Fig. 4(a). Here, $\beta \gtrsim \delta/E_J$ excludes the LZ transition. The probability behaves as $P_D \approx 1 - e^{-c\hbar\Gamma_D/eV}$, $c \sim \pi$ as the transition rate increases, in agreement with a Landau-Zener type argument, and is finite for $\hbar\omega_d \gtrsim \Delta - E_J$.

In the experimentally relevant [11] Shapiro step experiment, [23] the system is fed an additional ac current $I_r \sin(\omega_r t)$, and the 4π periodicity manifests as a kink in the dc-current-dc-voltage relation $\bar{I}(\bar{V})$ at $e\bar{V} = \hbar\omega_r$, whereas the first 2π step resides at $e\bar{V} = \hbar\omega_r/2$. Here, we assume the bias current $I_b(t) = \bar{I} + I_r \sin(\omega_r t) + I_d \sin(\omega_d t)$ contains a further high-frequency component $\omega_d \gg \omega_r$ which induces transitions to the continuum. To find the Shapiro steps we derive a semiclassical equation for the phase [23] by expanding the effective Keldysh action of the electromagnetic circuit in Fig. 1 to second order in quantum fluctuations φ^q, [17, 18, 24]

$$S[\varphi] \simeq -\frac{1}{e}\int_{-\infty}^{\infty} \mathrm{d}t\, [\frac{\hbar}{2eR}\dot{\varphi}^{cl}(t) - I_b(t) + I_J[\varphi^{cl}](t)]\varphi^q(t) \tag{7}$$

$$+\frac{i}{e^2}\int_{-\infty}^{\infty} \mathrm{d}t\, \mathrm{d}t'\, [\frac{k_B T\delta(t-t')}{R} + \frac{P_J[\varphi^{cl}](t,t')}{2}]\varphi^q(t)\varphi^q(t')\,.$$

The current $I_J(t) = \langle \hat{I}(t)\rangle$ and noise $P_J(t,t') =$

$\frac{1}{2}\langle\{\hat{I}(t),\hat{I}(t')\}\rangle$ functionals can in principle be obtained from the master equation. Considering the part $\frac{i}{e}\int_{-\infty}^{\infty}\mathrm{d}t'\,\theta(t-t')P_J[\varphi^{cl}](t,t')\varphi^q(t')$ in the last term as a mean field (well-defined on time scales longer than the relaxation/quasiparticle poisoning time), and assuming the effect of the junction on the phase dynamics is small ($I_J < \bar{I}_b$, $P_J < \bar{I}_b^2$), the saddle point becomes (c.f. Ref. 17)

$$\frac{1}{2R}\partial_t\varphi_*(t) + I_J[\varphi_*](t) + I_J^{(2)}[\varphi_*](t) = I_b(t)\,, \tag{8}$$

$$I_J^{(2)}[\varphi_*](t) \simeq \frac{-i}{e}\int_{-\infty}^{t}\mathrm{d}t'\,\mathrm{d}t''\,\frac{\delta P_J[\varphi_*](t,t')}{\delta\varphi(t'')}D^R(t'',t')\,. \tag{9}$$

The correlation function of the Ohmic environment circuit is $D^R(t,t') = -\frac{2ie^2R}{\hbar}\theta(t-t')$, $D^R(t,t) = 0$. The 4π periodic memory effects arise solely from the correlation function P_J, as the expectation value I_J must be invariant under translation $\varphi \mapsto \varphi + 2\pi$.

To find analytical results, we evaluate Eq. (8) in a simplified model retaining only the main physics (cf. Ref. 22): we neglect quantum coherence, and consider only the average populations $p_+ = \frac{\rho_{11,11}+\rho_{01,01}}{2}$, $p_- = \frac{\rho_{10,10}+\rho_{00,00}}{2}$ of the two upper and lower many-body states [see Fig. 2(d)]. The time evolution is constructed from LZ transitions $p_\pm \mapsto (1-P_{LZ})p_\pm + P_{LZ}p_\mp$ at $\varphi = \pi + 2\pi n$, and continuum relaxation $p_+ \mapsto (1-P_D)p_+$, $p_- \mapsto p_- + P_D p_+$ at $\varphi = 2\pi n$. Under this approximation, the I_J and P_J functionals can be found, [21] and the IV curve is obtained from the time average of Eq. (8).

First, continuum transitions increase the magnitude of the 2π Shapiro steps, as they remove quasiparticles from the low-energy levels. This is determined by the effective current–phase relation $I_J[\varphi](t)$. For slow or small deviations around the trajectory $\varphi(t) = 2\bar{V}t$, it can be approximated by the time-local relation $I_J(\varphi(t)) = \mathrm{Tr}\,\rho_0(\bar{V},\varphi(t))\hat{I}(\varphi(t))$ in the periodic steady state $\rho_0(\bar{V},\varphi) = \rho_0(\bar{V},\varphi+2\pi)$. We find ($\bar{V} > 0$)

$$I_J = I_c P_D \frac{(1-P_{LZ})\sin(\frac{\varphi}{2})\,\mathrm{sgn}(\cos(\frac{\varphi}{2})) + P_{LZ}|\sin(\frac{\varphi}{2})|}{1-(1-P_D)(1-2P_{LZ})}\,, \tag{10}$$

shown in Fig. 4(b). At low excitation $eRI_r/(\hbar\omega_r) \ll 1$ the resulting first Shapiro step at $2e\bar{V}/(\hbar\omega_r) = 1$ is similar to the supercurrent step at $\bar{V} = 0$, but with a smaller effective supercurrent $I_{c,1} = 2eRI_JI_r/(\hbar\omega_r)$. [29]

The 4π periodic features are contained in the time average $\overline{I_J^{(2)}} = \overline{I_{J0}^{(2)}} + \overline{\delta I_J^{(2)}}$. Here, $\overline{I_{J0}^{(2)}} \simeq RI_c^2/(2\bar{V})$, and the part $\overline{\delta I_J^{(2)}}$ proportional to I_r^2 is illustrated in Fig. 4(c). Increasing $P_D > 0$ cuts off the $e\bar{V} = \hbar\omega_r$ resonance in the IV curve.

For $P_{LZ} = 1$ and $P_D \to 0$ the correlation function factorizes, $P_J[\varphi](t,t') = I_c^2\sin(\varphi(t)/2)\sin(\varphi(t')/2)$, so that Eq. (7) can be transformed [24, 25] to the stochastic equation $\frac{\hbar}{2eR}\partial_t\varphi(t) + \mathcal{I}\sin(\varphi(t)/2) = I_b(t) + \xi(t)$ where $\mathcal{I}$ and the thermal noise $\xi(t)$ are Gaussian random variables. This result is also shown in Fig. 4 for comparison. Note that phase diffusion due to a finite temperature also suppresses the Shapiro steps, which is not taken into account in the figures.

Combining the steps from I_J and $I_J^{(2)}$, we obtain Fig. 4(d), which shows how the IV curve reflects the change in periodicity from 4π to 2π when P_D increases. This switching is tunable, and can be used to establish both the size of the gap $\Delta - E_J$ and the way the effect is directly related to the nonequilibrium state. Namely, in junctions with only 2π periodic Josephson effect, the high-frequency drive has no effect on the Shapiro steps within our model.

Summary. In summary, we consider microwave spectroscopy of Josephson junctions formed from hybridized Majorana bound states. We discuss what spectroscopic features manifest in a phase-biased situation, and how ac excitation can be used to tune the nonequilibrium state in the 4π periodic Josephson effect. High-frequency probing ($\hbar\omega_d \sim 400\,\mathrm{mK}\times k_B$) was achieved experimentally in Ref. 26 for superconducting quantum point contacts, and we expect high-frequency manipulation of junctions with Majorana bound states would also be feasible.

This work is supported by the Academy of Finland, DFG grant RE 2978/1-1 and the EU FP7 project SE2ND.

[1] A. Y. Kitaev, Physics-Uspekhi **44**, 131 (2001).
[2] H.-J. Kwon, K. Sengupta, and V. Yakovenko, EPJ B **37**, 349 (2004).
[3] L. Fu and C. L. Kane, Phys. Rev. B **79**, 161408 (2009).
[4] R. M. Lutchyn, J. D. Sau, and S. Das Sarma, Phys. Rev. Lett. **105**, 077001 (2010).
[5] F. Domínguez, F. Hassler, and G. Platero, Phys. Rev. B **86**, 140503 (2012).
[6] L. Jiang, D. Pekker, J. Alicea, G. Refael, Y. Oreg, and F. von Oppen, Phys. Rev. Lett. **107**, 236401 (2011).
[7] P. San-Jose, E. Prada, and R. Aguado, Phys. Rev. Lett. **108**, 257001 (2012).
[8] D. Pekker, C.-Y. Hou, V. Manucharyan, and E. Demler (2013), arXiv:1301.3161.
[9] P. San-Jose, J. Cayao, E. Prada, and R. Aguado (2013), arXiv:1301.4408.
[10] V. Mourik, K. Zuo, S. M. Frolov, S. R. Plissard, E. P. A. M. Bakkers, and L. P. Kouwenhoven, Science **336**, 1003 (2012).
[11] L. P. Rokhinson, X. Liu, and J. K. Furdyna, Nat. Phys. **8**, 795 (2012).
[12] A. Zazunov, V. S. Shumeiko, E. N. Bratus', J. Lantz, and G. Wendin, Phys. Rev. Lett. **90**, 087003 (2003).
[13] F. S. Bergeret, P. Virtanen, T. T. Heikkilä, and J. C. Cuevas, Phys. Rev. Lett. **105**, 117001 (2010).
[14] M. Zgirski, L. Bretheau, Q. Le Masne, H. Pothier, D. Esteve, and C. Urbina, Phys. Rev. Lett. **106**, 257003 (2011).

[15] T. L. Schmidt, A. Nunnenkamp, and C. Bruder (2012), arXiv:1211.2201.
[16] M. Trif and Y. Tserkovnyak, Phys. Rev. Lett. **109**, 257002 (2012).
[17] J. D. Sau, E. Berg, and B. I. Halperin (2012), arXiv:1206.4596.
[18] J. Michelsen and V. S. Shumeiko, Low Temp. Phys. **36**, 925 (2010).
[19] Y. Oreg, G. Refael, and F. von Oppen, Phys. Rev. Lett. **105**, 177002 (2010).
[20] J. D. Sau, R. M. Lutchyn, S. Tewari, and S. Das Sarma, Phys. Rev. Lett. **104**, 040502 (2010).
[21] For further details, see appendix.
[22] D. I. Pikulin and Y. V. Nazarov, Phys. Rev. B **86**, 140504 (2012).
[23] M. Tinkham, *Introduction to Superconductivity* (McGraw-Hill, New York, 1996), 2nd ed.
[24] U. Eckern, G. Schön, and V. Ambegaokar, Phys. Rev. B **30**, 6419 (1984).
[25] A. Kamenev and A. Levchenko, Adv. Phys. **58**, 197 (2010).
[26] M. Chauvin, P. vom Stein, D. Esteve, C. Urbina, J. C. Cuevas, and A. L. Yeyati, Phys. Rev. Lett. **99**, 067008 (2007).
[27] M. Cheng, R. M. Lutchyn, and S. Das Sarma, Phys. Rev. B **85**, 165124 (2012).
[28] For nanowire Hamiltonian $H_{BdG} = [-\frac{\hbar^2}{2m_*}\partial_x^2 - \mu + i\alpha\sigma_y\partial_x + V_x\sigma_x]\tau_z + \Delta_0\sigma_y\tau_+ + \Delta_0^*\sigma_y\tau_-$ in basis $(\psi_\uparrow, \psi_\downarrow, \psi_\uparrow^\dagger, \psi_\downarrow^\dagger)$ we take parameters $E_{so} = \alpha^2 m_*/(2\hbar^2) = 50\,\mu\mathrm{eV}$, $l_{so} = \hbar^2/(\alpha m_*) = 200\,\mathrm{nm}$, $L = 80 l_{so}$, $\Delta_0 = 1.7E_{so}$, $\mu = 1E_{so}$, $V_x = g\mu_B B_x = 10E_{so}$. The junction barrier is implemented by $\mu > \sqrt{V_x^2 - |\Delta_0|^2}$.
[29] Note that we assume a parameter regime outside the enhanced 4π locking effect discussed in Ref. 5. However, we expect the effect discussed here has a strong effect also in the locked regime.

Phenomenological rates

Quasiparticle poisoning (q), relaxation (r) and dephasing (d) can be described with the master equation Eq. (4) of the main text, by adding phenomenological rate terms: [7, 22]

$$\mathcal{L}_q\{\rho\} = \Gamma_q \sum_{k=-2}^{2} \mathcal{X}(d_k P)\{\rho\}\,, \tag{11}$$

$$\mathcal{L}_r\{\rho\} = \Gamma_r[\mathcal{X}(d_2 d_1) + \mathcal{X}(d_1^\dagger d_2)]\{\rho\}\,, \tag{12}$$

$$\mathcal{L}_d\{\rho\} = \Gamma_d \sin^2\!\big(\tfrac{\varphi}{2}\big) \sum_{k=1,2} \mathcal{X}(d_k^\dagger d_k)\{\rho\}\,, \tag{13}$$

$$\mathcal{X}(A)\{\rho\} \equiv A\rho A^\dagger - \frac{1}{2}[A^\dagger A, \rho]_+\,. \tag{14}$$

Similar terms can also be derived by integrating out a bosonic bath. [27] The dephasing rate is proportional to $|\partial_\varphi \epsilon_2(\varphi)|^2$, hence the phase dependence. Assuming QP poisoning time of order $1\,\mu$s and a Josephson energy of $E_J = 100\,\mathrm{mK}$, we have $\hbar\Gamma_q \simeq 10^{-4}E_J$. With environmental impedance $R \sim 1\,\Omega$, the relaxation rate Γ_r is also expected to be of a similar magnitude. [7] In the main text, we assumed the dephasing rate is $\hbar\Gamma_d = 10^{-3}E_J$. However, as long as $\hbar\Gamma_d \ll \hbar\omega_d, E_J$, dephasing affects the results here only slightly because they do not require quantum coherence.

Simplified master equation

Below, we discuss a simplified model, which describes the quasiparticle physics of the Andreev bound states on a semiclassical level. This enables us to obtain analytical results for the Shapiro steps, and we can compare its predictions to those of the more detailed microscopic model.

First, we assume the dephasing in the system is large enough, so that quantum coherence plays no role on time scales of $\hbar/(e\bar{V})$ (i.e. between two consequent Landau-Zener transitions). Under this assumption, the density matrix is projected as $\rho \mapsto \mathrm{diag}\,\rho$. Further, assuming that the lower and upper two many-body levels are equivalent (i.e., $\epsilon_1 \approx 0$) the system is described by the populations $p_+ = (\rho_{11,11} + \rho_{01,01})/2$ and $p_- = (\rho_{10,10} + \rho_{00,00})/2$. This defines a linear projection superoperator $P\{\rho\} = (p_+,\ p_-)^T$. Effect of Landau-Zener (LZ) and continuum (D) transitions can then be taken into account with projected propagators $U(t,t') = P\mathcal{T}e^{\int_{t'}^{t}\mathrm{d}t''\,\mathcal{L}(t'')}P^T$ of the master equation. For time evolution between $\varphi(t') = \pi - \beta \mapsto \varphi(t) = \pi + \beta$ and $\varphi(t) \mapsto \varphi(t'') = 3\pi - \beta$ with $\beta \sim \delta/E_J \ll 2\pi$ we have:

$$U_{LZ} \equiv PU(t,t')P^T \simeq \begin{pmatrix} 1-P_{LZ} & P_{LZ} \\ P_{LZ} & 1-P_{LZ} \end{pmatrix}, \quad U_D \equiv PU(t'',t)P^T \simeq \begin{pmatrix} 1-P_D & 0 \\ P_D & 1 \end{pmatrix}. \tag{15}$$

As a further simplification, we assume below that the continuum relaxation occurs instantaneously when the phase difference crosses the points $\varphi = 2\pi n$. The current superoperator $\hat{I}\{\rho\} = P\frac{e}{2\hbar}[\partial_\varphi H, \rho]_+ P^T$ in this representation is

$$\hat{I} \simeq \frac{e}{\hbar}\begin{pmatrix} \partial_\varphi \epsilon_2(\varphi) & 0 \\ 0 & -\partial_\varphi \epsilon_2(\varphi) \end{pmatrix} . \tag{16}$$

This allows straightforward approximation of the correlation functions required for the effective action.

Of importance here is the time evolution over a single period, $\varphi \mapsto \varphi + 2\pi$ (assuming $\varphi(t)$ is monotonically increasing):

$$U_c(\varphi) = U(\varphi + 2\pi, \varphi) = \begin{cases} U_D U_{LZ} , & 0 < \varphi < \pi \\ U_{LZ} U_D , & \pi < \varphi < 2\pi \end{cases} . \tag{17}$$

This determines the cyclic steady state $v_0 = P\{\rho_0\}$ of the system: $U_c(\varphi)v_0(\varphi) = v_0(\varphi)$, and the transient state $U_c(\varphi)v_1(\varphi) = \lambda_1 v_1(\varphi)$. Here, the decay factor for the transient state is $\lambda_1 = (1 - P_D)(1 - 2P_{LZ})$ and is independent of φ. Computing $I_J = \mathrm{Tr}\,\hat{I}\rho_0 = 1^T \hat{I} v_0$ we find Eq. (10) of the main text.

It is now convenient to define the projection superoperators $Q_0(\varphi) = v_0(\varphi)1^T$ and $Q_1(\varphi) = 1 - Q_0(\varphi)$ to the steady-state and transient subspaces. These satisfy $Q_0(\varphi)U_c(\varphi) = U_c(\varphi)Q_0(\varphi) = Q_0(\varphi)$, $Q_1(\varphi)U_c(\varphi) = U_c(\varphi)Q_1(\varphi) = \lambda_1 Q_1(\varphi)$, $Q_0(\varphi)^2 = Q_0(\varphi)$, and $Q_1(\varphi)^2 = Q_1(\varphi)$.

We assume the drive

$$\varphi_*(t) = \phi_0 + 2e\bar{V}t/\hbar + 2s_r[\cos(\omega_r t + \phi_r) - \cos(\phi_r)] . \tag{18}$$

When $e\bar{V}$ and $\hbar\omega_r$ are not exactly commensurate, long-time averages of periodic functions of $\varphi_*(t)$ can be computed by averaging over ϕ_0 and ϕ_r. The frequency component ω_d inducing the continuum transitions does not directly couple to the low-frequency dynamics, and is not included here for simplicity.

We can now evaluate the time-average of Eq. (9) of the main text under drive (18). First, we remark that $\frac{\delta}{\delta\varphi^{cl}(t'')} PU(t,t')P^T \approx 0$ within our approximations (see also Ref. 17). Moreover, $D^R(t,t) = 0$, so that only one term contributes in the expression

$$D^R(t'',t')\frac{\delta}{\delta\varphi^{cl}(t'')}\langle \hat{I}(t)\hat{I}(t')\rangle = D^R(t'',t')\langle (\partial_\varphi \hat{I})(t)\hat{I}(t')\rangle \delta(t - t'') . \tag{19}$$

Evaluating now the long-time average and changing integration variables, we find

$$\overline{I_J^{(2)}[\varphi_*](t)} = -2R\int_0^{2\pi}\frac{\mathrm{d}\phi_0}{2\pi}\int_0^{2\pi}\mathrm{d}\theta\ \mathrm{Tr}[(\partial_\phi \hat{I})(\theta+\phi_0)U(\theta+\phi_0,\phi_0)Q_1(\phi_0)\hat{I}(\phi_0)Q_0(\phi_0)]G(\theta) , \tag{20}$$

$$\begin{aligned} G(\theta) &= \frac{e}{\hbar}\sum_{m=0}^{\infty}\int_0^{2\pi}\frac{\mathrm{d}\phi_r}{2\pi}\frac{(1-P_D)^m(1-2P_{LZ})^m}{\partial_t\varphi_*(t_*(\theta+2\pi m,0,\phi_r))} \\ &= \frac{1}{2V}\frac{1}{1-(1-P_D)(1-2P_{LZ})} + \frac{(s_r\hbar\omega_r)^2}{4\bar{V}^3}\frac{\cos(\frac{\theta\hbar\omega_r}{2e\bar{V}}) - (1-P_D)(1-2P_{LZ})\cos(\frac{(2\pi-\theta)\hbar\omega_r}{2e\bar{V}})}{\sin(\frac{\pi\hbar\omega_r}{e\bar{V}})^2 + [\cos(\frac{\pi\hbar\omega_r}{e\bar{V}}) - (1-P_D)(1-2P_{LZ})]^2} + \mathcal{O}(s_r^4) . \end{aligned} \tag{21}$$

The function $t_*(\theta,\phi_0,\phi_r)$ is defined by $\varphi_*(t_*(\theta,\phi_0,\phi_r)) = \theta$.

All information about the 4π periodicity and the drive is contained in the factor $G(\theta)$. For $P_{LZ} = 0$, the maximum amplitude is obtained when the drive is 2π periodic in θ, and for $P_{LZ} = 1$ when it is 4π periodic. Moreover, $P_D > 0$ suppresses correlations between cycles, and cuts them off completely at $P_D = 1$.

Equation (20) can be evaluated analytically, in the leading order in the drive amplitude s_r. In the interesting case

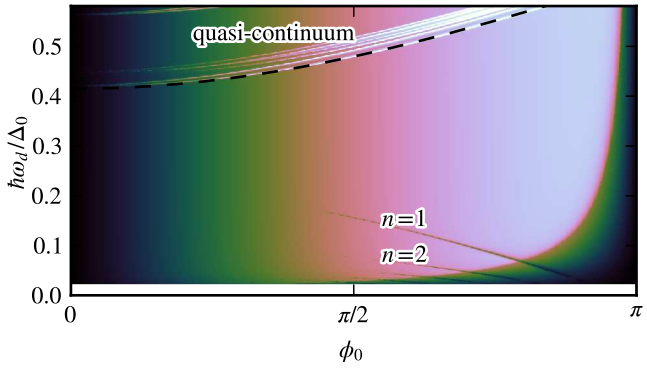

FIG. 5: Time-averaged current-phase relation for a nanowire system. As Fig. 3 in the main text, but for the nanowire system whose spectrum and connections are displayed in Fig. 2, corresponding to parameters given in [28]. The wire was chosen long, so that the energy splittings $\delta_\pm$ of the Majorana states are small, and the resonances corresponding to transitions between the low-lying bound states are weak. They are more pronounced in shorter wires, as illustrated in Fig. 2 of the main text. Resonances associated with transitions to continuum levels are not similarly suppressed. The assumed continuum inverse lifetime is $\Gamma_0/E_J = 10^{-3}$.

of $P_{LZ} = 1$, we obtain

$$\overline{I_J^{(2)}} = \overline{I_{J,0}^{(2)}} + \overline{\delta I_J^{(2)}} + \mathcal{O}(s_r^4) \tag{22}$$

$$\overline{I_{J,0}^{(2)}} = \frac{2(1-P_D)[(4-\pi)P_D + 2\pi]}{(2-P_D)^3\pi}\frac{RI_c^2}{\bar{V}} \tag{23}$$

$$\begin{aligned}(eR)^{-1}I_c^{-2}\overline{\delta I_J^{(2)}} = &-\frac{2(1-P_D)P_D^2 s_r^2(\hbar\omega_r)^3\sin\left(\frac{\pi\hbar\omega_r}{e\bar{V}}\right)}{\pi(P_D-2)^2(e\bar{V}-\hbar\omega_r)^2(e\bar{V}+\hbar\omega_r)^2\left(P_D^2 - 2P_D\cos\left(\frac{\pi\hbar\omega_r}{e\bar{V}}\right) - 2P_D + 2\cos\left(\frac{\pi\hbar\omega_r}{e\bar{V}}\right) + 2\right)} \\ &- \frac{4(1-P_D)P_D s_r^2(\hbar\omega_r)^2\cos\left(\frac{\pi\hbar\omega_r}{2e\bar{V}}\right)}{\pi(P_D-2)e\bar{V}(e\bar{V}-\hbar\omega_r)(e\bar{V}+\hbar\omega_r)\left(P_D^2 - 2P_D\cos\left(\frac{\pi\hbar\omega_r}{e\bar{V}}\right) - 2P_D + 2\cos\left(\frac{\pi\hbar\omega_r}{e\bar{V}}\right) + 2\right)} \\ &+ \frac{(1-P_D)s_r^2(\hbar\omega_r)^2}{(P_D-2)^2 e\bar{V}(e\bar{V}-\hbar\omega_r)(e\bar{V}+\hbar\omega_r)}\,.\end{aligned} \tag{24}$$

This result is plotted in Fig. 4 of the main text. Note that it applies in the limit where the junction has a small effect on the dynamics of the phase φ — that is, Eq. (18) is valid. Divergences (e.g. $\bar{V} \to 0$) indicate a breakdown of this approximation.

Discrete continuum spectrum

The level spacing in the continuum part of the energy spectrum in nanowires is not necessarily small, for instance in a proximity nanowire setup where the effective energy gap Δ in the nanowire is smaller than the gap Δ_S of the proximity superconductor inducing it. Our main results apply also in this case — Figs. 5 and 6 show that only limited qualitative changes are expected from the discreteness of the continuum spectrum.

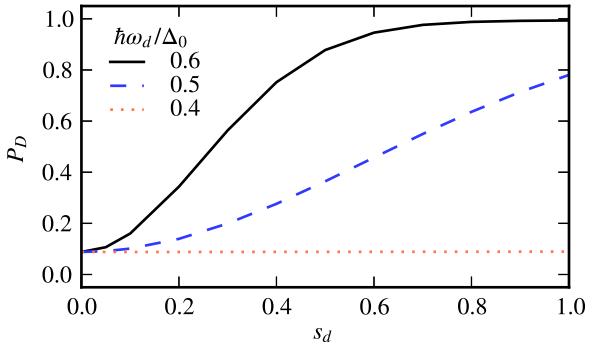

FIG. 6: Probability of continuum relaxation for a nanowire system. As Fig. 4(a) in the main text, but for the nanowire system whose spectrum and connections displayed in Fig. 2, and shown as a function of s_d with fixed $eV = 0.01E_J$. The offset from zero is due to a finite spontaneous quasiparticle poisoning and relaxation with rates $\Gamma_{r,q}/E_J = 10^{-4}$. The result is not sensitive to continuum lifetime Γ_0^{-1}.